CFD Modeling and LDA Measurements for the Air-Flow in an Aero Engine Front Bearing Chamber

J. Aidarinis

D. Missirlis

K. Yakinthos

A. Goulas

Laboratory of Fluid Mechanics and Turbomachinery,
Department of Mechanical Engineering,
Aristotle University of Thessaloniki,
Egnatia Street,
54124 Thessaloniki, Greece

The continuous development of aero engines toward lighter but yet more compact designs, without decreasing their efficiency, has led to gradually increasing demands on the lubrication system, such as the bearing chambers of an aero engine. For this reason, it is of particular importance to increase the level of understanding of the flow field inside the bearing chamber in order to optimize its design and improve its performance. The flow field inside a bearing chamber is complicated since there is a strong interaction between the sealing air-flow and the flow of lubrication oil, and both of them are affected by and interacting with the geometry of the chamber and the rotating shaft. In order to understand the flow field development and, as a next step, to optimize the aero engine bearing chamber performance, in relation to the lubrication and heat transfer capabilities, the behavior of this interaction must be investigated. In this work, an investigation of the air-flow field development inside the front bearing chamber of an aero engine is attempted. The front bearing chamber is divided into two separate sections. The flow from the first section passes through the bearing and the bearing holding structure to the second one where the vent and the scavenging system are located. The investigation was performed with the combined use of experimental measurements and computational fluid dynamics (CFD) modeling. The experimental measurements were carried out using a laser Doppler anemometry system in an experimental rig, which consists of a 1:1 model of the front bearing chamber of an aero engine. Tests were carried out at real operating conditions both for the air-flow and for the lubricant oil-flow and for a range of shaft rotating speeds. The CFD modeling was performed using a commercial CFD package. Particularly, the air-flow through the bearing itself was modeled, adopting a porous medium technique, the parameters of which were developed in conjunction with the experiments. A satisfactory quantitative agreement between the experimental measurements and the CFD computations was achieved. At the same time, the effect of the important parameters such as the air and oil mass flow, together with the shaft rotational speed, and the effect of the chamber geometry were identified. The conclusions can be exploited in future attempts in combination with the CFD model developed in order to optimize the efficiency of the lubrication and cooling system. The latter forms the main target of this work, which is the development of a useful engineering tool capable of predicting the flow field inside the aero engine bearing, which can be used subsequently for optimization purposes. [DOI: 10.1115/1.4002830]

Keywords: bearing chamber, aero engine, air-oil-flow, porous media, CFD

1 Introduction

To a large extent, the design of bearing chambers has been based on empirical correlations derived from research and knowledge gathered through years of experience and from time consuming experiments. The development of aero engines is now focused toward lighter and more compact designs, which put increasing demands on the lubrication system. Since the increase in engine thermal efficiency demands an increase in turbine inlet temperature, turbine blades encounter a higher input temperature and, additionally, the cooling air taken from the compressor with the use of an internal air system and guided to the bearing chamber is also at a higher temperature. The latter leads to a reduction of the temperature difference and thus, to a deterioration of the cooling process. To compensate for this problem, larger amounts of air mass flow are required for the cooling of the lubrication system. This unfortunately leads to a power loss of the engine, especially if the increase in cooling requirements leads to larger pumps, heat exchangers, and filters, thus adding extra weight and unavoidably leading to higher engine power requirements. Regarding the oil-flow through a bearing compartment, only a relatively small part of the oil is used to lubricate the bearings, while most of the oil is used to provide sufficient cooling capability. For these reasons, a sufficient assessment of the flow in the bearing chamber regarding the internal air-flow and lubrication system is of particular importance when the aero engine performance is investigated.

1.1 Background. Studies by Willenborg et al. [1] into bearing chambers have examined the heat transfer characteristics with specific focus on oil fires and engine coking problems. Ignition mechanisms were identified and a strong dependence on the air/oil mixture characteristics was concluded. Earlier investigations by Wittig et al. [2] into bearing chamber flows dealt mainly with the use of an ultrasonic film thickness measurement technique. It was demonstrated that the heat transfer characteristics depended on the

Contributed by the International Gas Turbine Institute (IGTI) of ASME for publication in the JOURNAL OF ENGINEERING FOR GAS TURBINES AND POWER. Manuscript received July 6, 2010; final manuscript received July 19, 2010; published online April 8, 2011. Editor: Dilip R. Ballal.

rotational speed and the mass flow of oil into the chamber. An extension of this work was carried out by Glahn et al. [3] to include film velocity measurements where the air flow regime is fundamental to the calculation procedure of film flows. Oil droplet flow investigations from Glahn et al. [4] also showed a strong dependence of the oil phase motion on the air flow. The strength of the secondary air flow and recirculation regions ensuing in the complex shape could have an effect on the flow of the oil in the form of droplets. Droplet size distributions and droplet entrainment from oil films were also identified by Glahn et al. [5]. It was shown that the dispersed oil phase is greatly affected by the air phase flow patterns, which have an implication on the lubrication and cooling of bearing chambers. In these studies, the authors employed only a numerical procedure to calculate the air flow and concluded that any successful numerical analysis of two-phase flow phenomena in bearing chambers requires a thorough understanding of the air flow in order to derive a relation for the coupling between the air and oil phase flows.

In addition, Busam et al. [6] carried out measurements for the heat transfer characteristics and attempted to present a generalized description of the heat transfer in a bearing chamber. Various parameters such as chamber height, rotational speed, and lubrication oil-flow were examined. Jakoby et al. [7] studied the air-flow in a simplified chamber consisting of two coaxial cylinders.

Wang et al. [8] and Farrall et al. [9,10] presented a modeling work aiming to provide an insight into bearing chamber flows, but experimental data are still required to substantiate these results. Finally, Lee at al [11] carried out investigations using particle image velocimetry measurements of the air-flow and presented CFD modeling results for a rig, simulating the high pressure-intermediate pressure bearing chamber, which were in reasonable agreement with the experimental results.

A thorough understanding of the single-phase flow features will provide valuable insight into the subsequent effects of two-phase flow transport and heat transfer effects. Such an effort is presented in this work where the air-flow inside the bearing chamber of an aero engine is investigated. The main aim of this attempt is to increase the level of understanding of the flow field inside the bearing chamber, in order to be able to optimize at a latter stage its design and performance. Since the flow field in such cases is complicated, there is a strong interaction between air-flow and lubrication oil-flow strongly affected by the shaft rotational speed and the geometry of the bearing chamber itself. The way this interaction takes place must be investigated in order to understand the flow field development and, at a next step, to optimize its performance.

The investigation was performed with the combined use of experimental measurements and CFD modeling. The experimental measurements were carried out with the use of a laser Doppler anemometry (LDA) system in an experimental rig, modeling the bearing chamber of an aero engine under various operating conditions taking into account both air-flow and lubrication oil-flow and for a varying number of shaft rotational speeds. The CFD modeling was performed with the use of the commercial CFD package FLUENT 12 [12], while for the turbulence modeling a Reynolds stress model (RSM) was used. The air-flow inside the bearing was modeled with the adoption of a porous medium methodology. In this approach, the precise geometry of the bearing itself is not modeled but its effect on the pressure losses is described as a function of the air-flow velocity, which is added as a source term in the momentum equations. It must be mentioned that in this investigation even though the experimental measurements were carried out with the use of air-flow and lubrication oil-flow, in the CFD computations only the air-flow was studied. The main target of this work is to generate an engineering computational tool, which would be possible to use as a further step for optimization purposes.

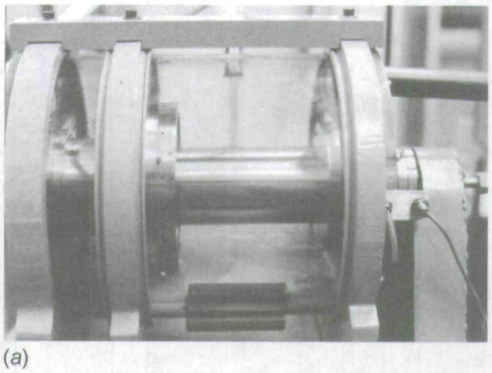

(*a*)

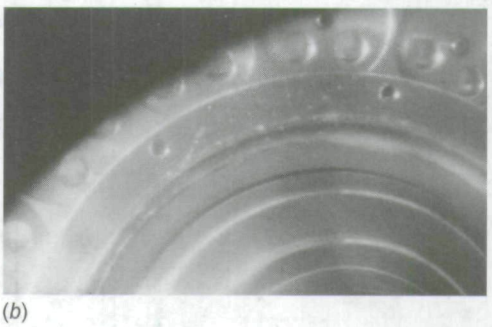

(*b*)

Fig. 1 Bearing chamber test rig (*a*) general view and (*b*) enlarged view in the bearing cage region

2 Experimental Setup

In order to proceed to the experimental measurements, a 1:1 scale test rig of an aero engine bearing chamber was designed and constructed, as presented in Figs. 1 and 2.

The bearing chamber is divided into two distinct regions, the front bearing region located at the left of the bearing and the rear bearing region located to the right. These two regions are con-

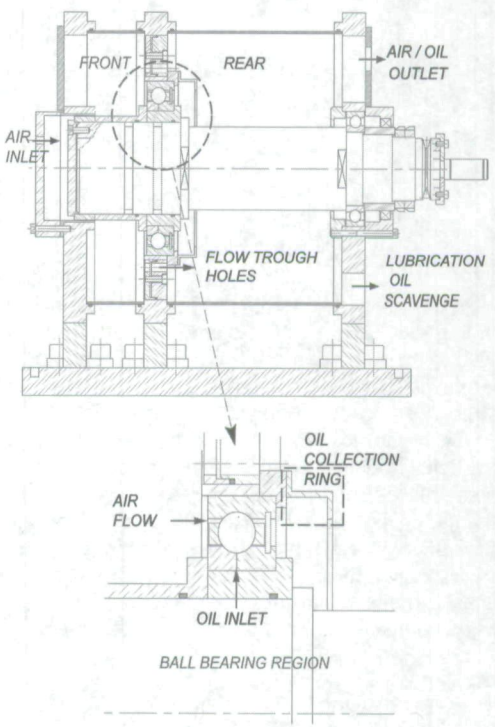

Fig. 2 Bearing chamber test rig cross section design

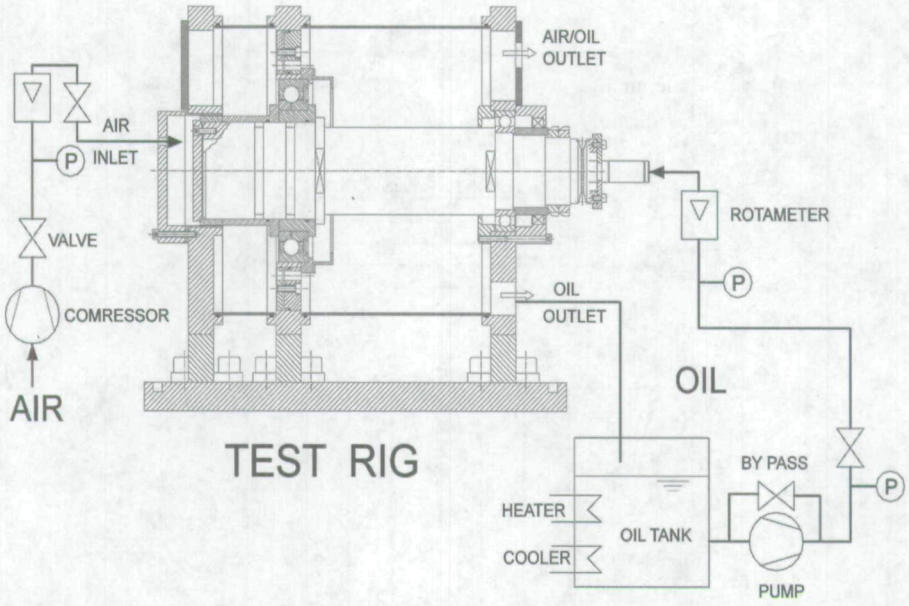

Fig. 3 Bearing chamber experimental test facilities

nected with each other through 32 small holes (∅10 mm), as shown in Fig. 2. The air-flow enters the bearing chamber through a small entrance ring region simulating the labyrinth seal and moves into the front region of the bearing. Then, the air-flow is split, and one part passes through the small holes and moves toward the back region of the bearing while the other part goes through the 2 mm gap between the bearing cage and the outer ring, as shown in the enlarged view in Fig. 2, toward the back region of the bearing chamber. The amount of air-flow passing through the ball bearing region depends on the flow conditions and the rotational speed of the shaft, and it is an important parameter that must be considered in the investigation.

At real operating conditions the flow inside the bearing is a two-phase flow since lubrication oil is inserted in the bearing cage for lubrication reasons. A schematic representation of the test facility is presented in Fig. 3.

The bearing chamber has cylindrical Perspex walls allowing for optical access. The dimensions of the front (upstream) and the rear (downstream) sections of the bearing chamber are presented in Table 1.

The shaft is supported on one end by a small bearing with a separate sealed lubrication system and on the other end by the main bearing of the chamber. The ball bearing had an internal diameter of ∅125 mm and external diameter of ∅190 mm and requires an under-race lubrication system.

The shaft itself was hollow. The shaft was plugged at the end of the air-flow intake, labyrinth seal side. At the other side of the shaft, a small pipe was connected, through which the lubrication oil was supplied. This small pipe was stationary and was fitted into the end of the rotating shaft.

Table 1 Bearing chamber dimensions

Height of front chamber	h_F (mm)	95
Height of rear chamber	h_R (mm)	105
Width of front chamber	w_F (mm)	70
Width of rear chamber	w_R (mm)	205
Diameter of vent port	d_V (mm)	25
Diameter of scavenge port	d_S (mm)	25
Radius of front shaft	r_F (mm)	110
Radius of rear shaft	r_R (mm)	90
Diameter of holes	d_p (mm)	10

Special self-lubricating small ball bearings were used to allow rotation, acting also as O-rings in order to avoid any leakage between the small pipe and the end of the shaft.

3 LDA Measurements

LDA is a widely and commonly used technique for flow investigations due to unambiguous advantages given by the nonintrusive measurements and by the fact that it is comparatively insensitive to pressure and temperature fluctuations. In this work, LDA measuring system was used to measure the air-flow through the bearing chamber. The small droplets produced from the oil coming through the bearing are mixed with the air and were used as seeding particles. Oil droplets of the size range between 1 μm and 10 μm usually follow the air-flow without slip and are regarded as ideal seeding particles. Larger droplets, which do not follow the flow, were prevented from entering the flow field by using a specially designed collection ring. Large droplets, which escaped the collection system, produced scattered light signal, were ignored using the proper signal filtration ranges in the burst spectrum analyzer (BSA) setup. The laser Doppler anemometry measurement equipment used for the experimental measurements was made by Dantec.

This system is a back scattering 2D system consisting of the following items:

(i) an argon-ion laser source, Spectra-Physics model 2020-3 with a power of 3 W
(ii) a fiber optic link with the necessary optical manipulators for the transfer of the laser beam from the source to the optics

Table 2 Measurement conditions

Type of oil	Mobil Jet II
Rotational speed (n (rpm))	4000, 5500, 7000
Oil-flow ($\dot{V}_l$ (l/h))	150
Sealing air-flow ($\dot{m}_g$ (g/s))	23, 33
Air temperature ($T_{g,in}$ (K))	300
Oil temperature ($T_{l,in}$ (K))	333
Chamber pressure (p_i (kPa))	3–4

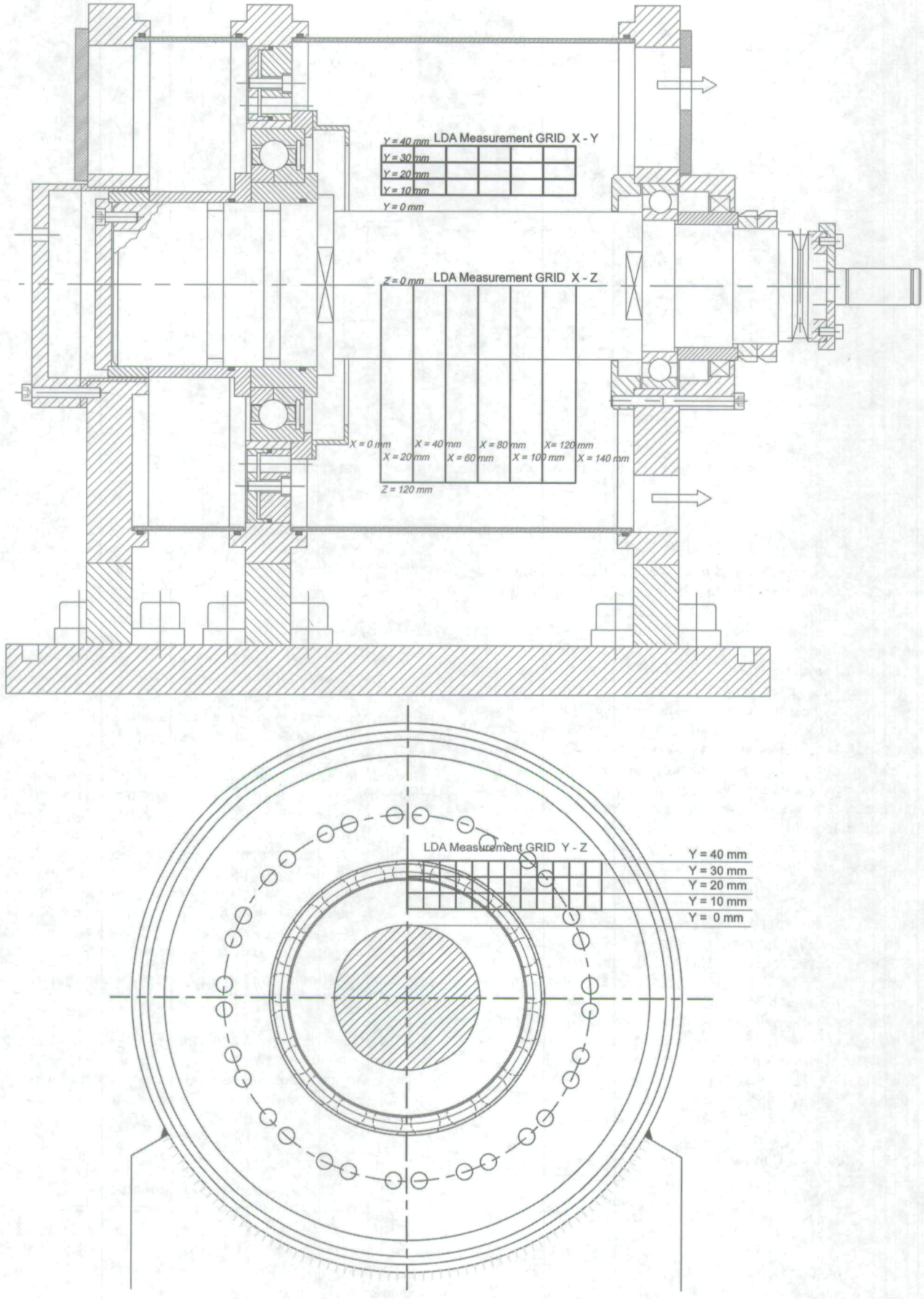

Fig. 4 Measurement position inside the bearing chamber

(iii) transmitting and receiving optics Dantec 55X (f=310) with 40 MHz Bragg-cell, beam separator, and color separator
(iv) a backscatter detecting system with two photomultipliers
(v) a frequency shifting system to identify the sign of velocity (Dantec 55L11, 55L12)
(vi) a BSA (Dantec 57N21, 57N56P)
(vii) a PC for storage and data processing running the BSA flow software

The whole system was supported on an X-Y traversing table with an accuracy of positioning of 0.001 mm made by Newport model MTL 250PP1 and driven by a Newport M4000 controller.

The system was used only to obtain the axial component of velocity due to limitations mainly set by the experimental test rig wall curvature.

4 Cases Studied

Measurements were carried out at operational conditions corresponding to shaft rotational speed of 4000 rpm, 5500 rpm, and 7000 rpm. Two air-flow rates, 23 g/s and 33 g/s, were examined while the oil-flow rate was kept constant and was equal to 150 l/h. Details can be found in Table 2.

The measurements were carried out only at the top half of the chamber downstream of the bearing in order to avoid reflection problems from the shaft since the laser beams should pass through the chamber from one side to the other without interruption from high reflecting parts such as the metal surfaces of the shaft or the supporting plates.

The main problem encountered was the formation of the oil film on the bearing chamber wall. The oil film, due to its irregular interface with the air could diffract the laser beams and cause a very bad signal to noise ratio making the acquisition of the data almost impossible. To alleviate the problem, a special oil collection ring, which prevented the oil droplets produced from the bearing in reaching the wall, was installed, as shown in Fig. 2.

A similar situation was described also by Flouros [13], who conducted experiments in a bearing compartment using a ball bearing of an aero engine. He concluded that the amount of droplets generated by the ball bearing is reduced when using porous screens to surround the bearing. Visualization of the bearing with a high-speed camera showed that much less spray was produced when the bearing was surrounded by screens.

The measurement domain is presented in Fig. 4 and ranges to

- Z direction (0–120 mm) measured on a meridional plane starting from the shaft toward the wall with a step of 10 mm
- Y direction (10–40 mm) measured on a horizontal plane, zero being on the shaft (and the value increases toward the wall with a step of 10 mm)
- X direction (20–140 mm) along the axis starting from the oil collection ring toward the rear plate

The measured points were limited to

- Z$\Leftarrow$120 mm due to the increase of the noise produced from the reflection and the refraction of the laser beams close to the Perspex wall
- Y$\Leftarrow$40 due to the increasing curvature of the Perspex wall, which causes higher refraction angle of the laser beams as they pass through the wall
- X$\Rightarrow$20 due to the angle between the laser beams (30 deg)

5 CFD Modeling of the Bearing Chamber

For the CFD modeling, a 3D computational model of the whole bearing chamber was generated with the use of GAMBIT [14] CFD software. Typical views of the computational domain and the computational grid are presented in Figs. 5 and 6. The CFD computations were performed with the use of the FLUENT CFD commercial software.

Regarding the boundary conditions, at the inlet of the computational domain the air mass flow was prescribed with the ratio of the axial velocity to the tangential velocity being set equal to 9, following the suggestions of Gorse et al. [15] regarding the azimuthal velocity of the air at which the exit of the labyrinth ranges between 20% and 30% of the shaft speed. At the outlet of the computational domain, the static pressure was set equal to the value obtained from the experimental measurements. In addition, the shaft rotational speed was set each time as in the experimental measurements. The rotational speed of the bearing cage was calculated from the geometric characteristics of the bearing and was set at 1772 rpm, 2436 rpm, and 3101 rpm for the corresponding rotational speed of the shaft 4000 rpm, 5500 rpm, and 7000 rpm.

CFD computations were performed for air at a temperature of 300 K. At the outlet, the absolute pressure was set equal to the value obtained by the measurements ranging from 104,100 Pa for air-flow of 23 g/s to 105,600 Pa for air-flow of 33 g/s. The flow was computed as a compressible one. The computational grid consisted of 915,856 computational cells. Additional computations were carried out with grids of 1.5×10^6 and 0.5×10^6 computational points in order to estimate the grid independency of the CFD results. For the turbulence modeling, the RSM [16] was used.

The second-order upwind discretization scheme was selected. Standard wall functions were employed where the y^+ values at the walls were between 11.25 and 100 to ensure the validity of the application of the logarithmic law-of-the-wall.

At the first steps of the computations, the rotation speed of the shaft was set to a zero value and after some iterations the rotational shaft speed was gradually increased until it reached the

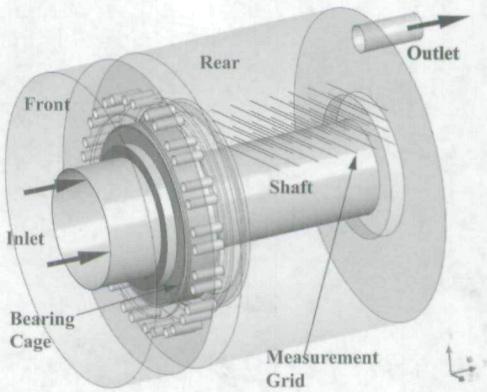

Fig. 5 Computational domain and measurement grid position inside the bearing chamber

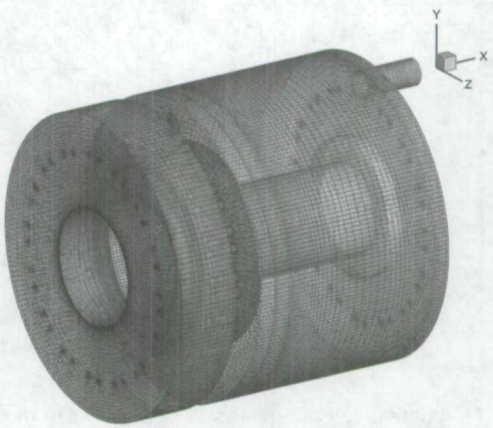

Fig. 6 Bearing chamber computational grid

selected value. Furthermore, at the first steps of the computations the standard k−ε model was used as the initial solution for the RSM model.

In the CFD model the outer ball bearing cage gap was modeled as a porous medium zone with a predefined pressure drop law which was initially selected in the form of Eq. (1). This equation is similar to the inertial part of the Darcy–Forchheimer pressure drop law equation, which is one of the most commonly used formulations presented in the international literature,

$$\frac{\partial P}{\partial x_i} = C_i \frac{1}{2} \rho U_i^2 \tag{1}$$

The main advantage of this approach is the significant reduction of the number of computational points which would otherwise be required in case that the precise ball bearing region had to be modeled. However, the use of a porous medium methodology requires a proper selection of both the form of the pressure drop law and of the pressure loss coefficient values. The prescribed pressure drop law has an important effect in the amount of air that passes through the ball bearing region. The higher the pressure loss is, the higher the flow resistance through the ball bearing region becomes and vice versa.

For the derivation of the proper pressure loss coefficient in this work, the LDA experimental measurements that have been carried out were used and through a trial-and-error procedure various values of the pressure loss coefficient were applied and CFD computations were performed. After some efforts, in each case the optimum pressure loss coefficient value for which the CFD results were in close agreement with the experimental measurements, as presented in Fig. 7, was selected.

Typical plots of the CFD computations and the flow field development are presented in Fig. 8. Figure 8 shows that the air-flow exits through the small holes in a way similar to that of a jet-flow. In addition, the amount of air-flow passing through the bearing has a strong swirl. These two air-flow streams interact with each other and move toward the vent outlet exit having a circumferential velocity. As a result, a large recirculation region with a strong swirl is developed close to the rotation shaft, which extends up to the bearing inner ring.

Figure 7 shows that the CFD results are in satisfactory agreement with the LDA measurements. However, as long as a trial-and-error procedure was used for the proper selection of the pressure loss coefficient, the relationship developed here might not be easily applicable for cases where experimental measurements are not available. For this reason, it was necessary to derive a more generalized pressure drop formulation in order to be able to perform CFD computations for optimization reasons. Furthermore, since the optimum pressure loss coefficient values varied from case to case, this was a strong indication that the initially used pressure drop formulation might have to be reconsidered. Thus, the CFD results were analyzed and the values presented in Table 3, which were corresponding to static pressure drop between the inlet and outlet region of the porous medium (outer ball bearing cage gap) and the air-flow in the bearing chamber and the shaft rotational speed were derived.

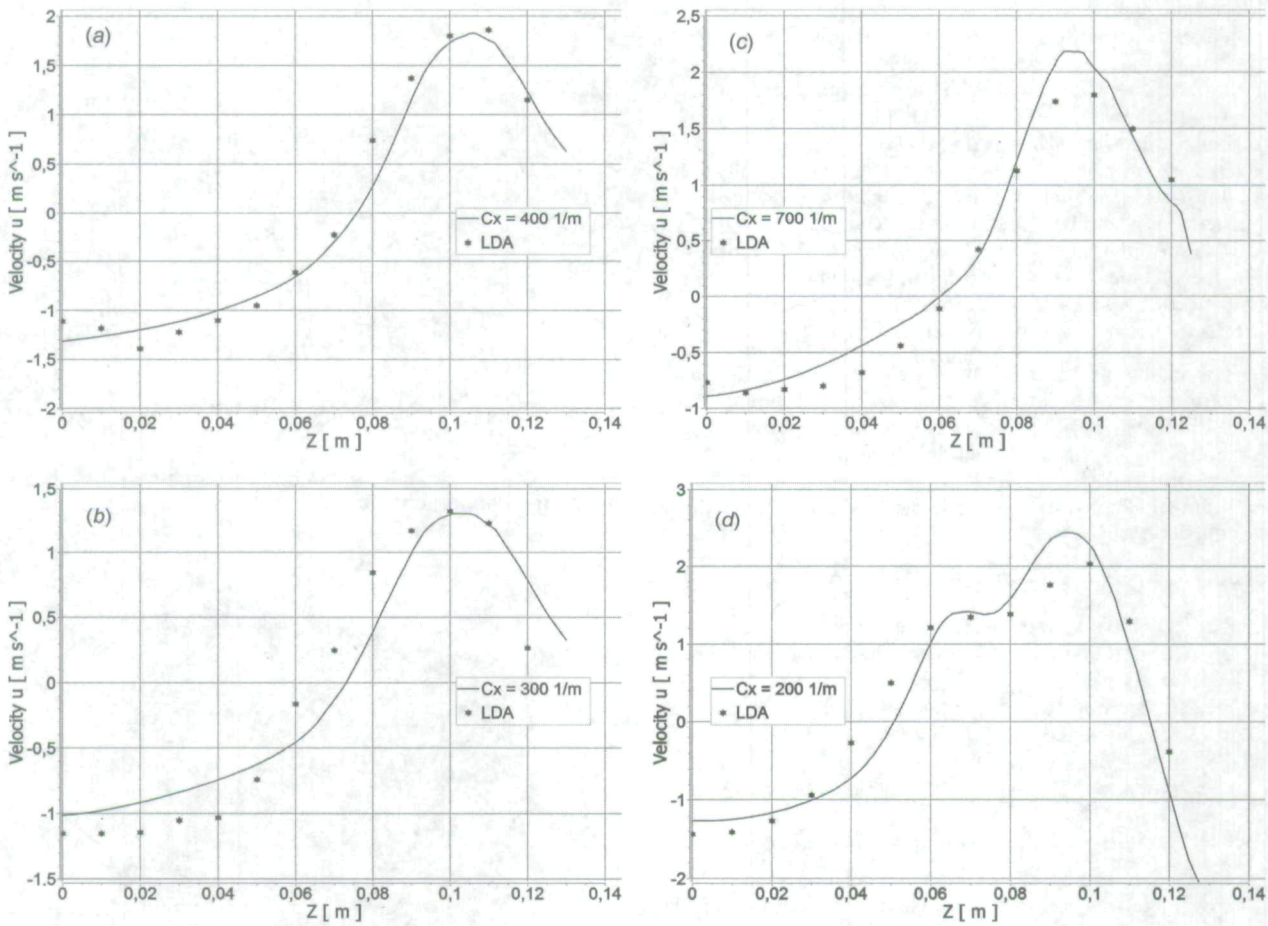

Fig. 7 Axial velocity comparison between LDA measurements and CFD results. (*a*) 5500 rpm, mg=33 g/s, x=163.5 mm, and y=55 mm. (*b*) 4000 rpm, mg=23 g/s, x=163.5 mm, and y=55 mm. (*c*) 4000 rpm, mg=33 g/s, x=163.5 mm, and y =75 mm. (*d*) 5500 rpm, mg=23 g/s, x=143.5 mm, and y=55 mm.

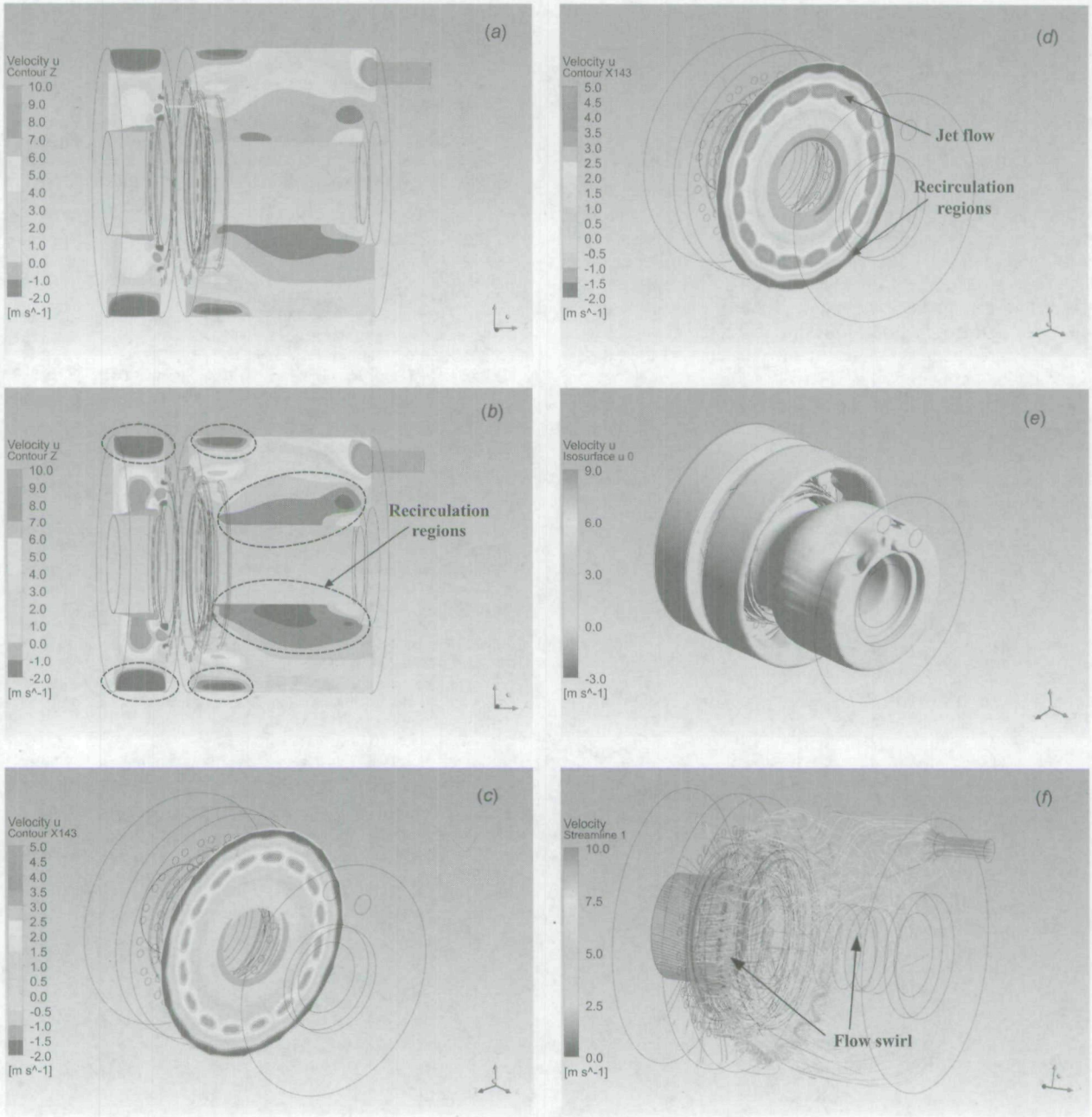

Fig. 8 Typical plots of the CFD computations. (*a*) Axial velocity contour 4000 rpm and mg=23 g/s. (*b*) Axial velocity contour 5500 rpm and mg=33 g/s. (*c*) Axial velocity contour 4000 rpm and mg=23 g/s. (*d*) Axial velocity contour 5500 rpm and mg=33 g/s. (*e*) Negative velocity isosurfaces 4000 rpm and mg=23 g/s. (*f*) Velocity magnitude streamlines 5500 rpm and mg=33 g/s.

Table 3 CFD results between the inlet and the outlet of the porous medium

Dp_{st} (Pa)	$\dot{m}_g$ (g/s)	n (rpm)
193	23	4000
174	23	5500
148	23	7000
395	33	4000
386	33	5500
349	33	7000

From the analysis of the CFD results, it was shown that the use of a pressure drop law in the form presented in Eq. (2) would provide a R^2 value of 0.999,

$$\frac{\partial P}{\partial x} = a + b\dot{m}_g + cn + dn^2 \tag{2}$$

where the values a, b, c, d are constants.

The use of the more generalized pressure drop formulation can accurately describe the pressure drop in the outer ball bearing cage gap in a more complete way since no trial-and-error procedure is required for the calculation of the pressure loss coefficients and thus providing the possibility to use the overall CFD model in an optimization effort.

6 Conclusions

In the present work, the investigation of the flow in the bearing chamber of an aero engine is performed with the use of experimental measurements and CFD computations. For the CFD computations, only the air-flow inside the bearing chamber was considered. The air-flow through the bearing cage itself was included in the solution by adopting a porous medium model. The experimental measurements and the CFD computations presented similar flow patterns and have satisfactory agreement. Furthermore, the effect of important parameters such as the air and oil mass flow and the shaft rotational speed and the effect of the chamber geometry were identified. A porous medium pressure drop model was developed to simulate the effect of the bearing itself on the air-flow through the chamber. This specific approach can be exploited in future attempts to increase the efficiency of the lubrication and cooling system.

Nomenclature

C_i = pressure loss coefficient
d_P = diameter of holes
d_S = diameter of scavenge port
d_V = diameter of vent port
h_F = height of front chamber
h_R = height of rear chamber
$\dot{m}_g$ = air-flow
n = rotational speed
P = static pressure
p_i = chamber relative pressure
$T_{g,in}$ = air temperature
$T_{l,in}$ = oil temperature
r_F = radius of front shaft
r_R = radius of rear shaft
$\dot{V}_l$ = oil-flow
U_i = i-velocity component
w_F = width of front chamber
w_R = width of rear chamber

Greek Symbols

ρ = density

References

[1] Willenborg, K., Busam, S., Roßkamp, H., and Wittig, S., 2002, "Experimental Studies of the Boundary Conditions Leading to Oil Fire in the Bearing Chamber and in the Secondary Air System of Aeroengines," ASME Turbo Expo, Amsterdam, The Netherlands.

[2] Wittig, S., Glahn, A., and Himmelsbach, J., 1994, "Influence of High Rotational Speeds on Heat Transfer and Oil Film Thickness in Aero-Engine Bearing Chambers," ASME J. Eng. Gas Turbines Power, **116**, pp. 395–401.

[3] Glahn, A., and Wittig, S., 1996, "Two-Phase Air/Oil-Flow in Aero Engine Bearing Chambers: Characterization of Oil Film Flows," ASME J. Eng. Gas Turbines Power, **118**, pp. 578–583.

[4] Glahn, A., Kurreck, M., Willmann, M., and Wittig, S., 1996, "Feasibility Study on Oil Droplet Flow Investigations Inside Aero Engine Bearing Chambers-PDPA Techniques in Combination With Numerical Approaches," ASME J. Eng. Gas Turbines Power, **118**, pp. 749–755.

[5] Glahn, A., Busam, S., Blair, M. F., Allard, K. L., and Wittig, S., 2002, "Droplet Generation by Disintegration of Oil Films at the Rim of a Rotating Disk," ASME J. Eng. Gas Turbines Power, **124**, pp. 117–124.

[6] Busam, S., Glahn, A., and Wittig, S., 2000, "Internal Bearing Chamber Wall Heat Transfer as a Function of Operating Conditions and Chamber Geometry," ASME J. Eng. Gas Turbines Power, **122**, pp. 314–320.

[7] Jakoby, R., Kim, S., and Wittig, S., 1999, "Correlations of the Convection Heat Transfer in Annular Channels With Rotating Inner Cylinder," ASME J. Eng. Gas Turbines Power, **121**, pp. 670–677.

[8] Wang, Y., Hibberd, S., Simmons, K., Eastwick, C., and Care, I., 2001, "Application of CFD to Modelling Two-Phase Flow in a High-Speed Aero-Engine Transmission Chamber," ASME Fluids Engineering Division Summer Meeting, New Orleans, LA.

[9] Farrall, M., Hibberd, S., and Simmons, K., 2003, "Modelling Oil Droplet/Film Interaction in an Aero-Engine Bearing Chamber," ICLASS, Sorrento, Italy.

[10] Farrall, M. B., Hibberd, S., and Simmons, K., 2000, "Computational Modelling of Two-Phase Air/Oil-Flow Within an Aero-Engine Bearing Chamber," ASME Fluids Engineering Division Summer Meeting, Boston, MA.

[11] Lee, C. W., Palma, P. C., Simmons, K., and Pickering, S. J., 2005, "Comparison of Computational Fluid Dynamics and Particle Image Velocimetry Data for the Airflow in an Aeroengine Bearing Chamber," Trans. ASME: J. Eng. Gas Turbines Power, **127**, pp. 697–703.

[12] ANSYS FLUENT 12.0 Documentation.

[13] Flouros, M., 2006, "Reduction of Power Losses in Bearing Chambers Using Porous Screens Surrounding the Ball Bearing," ASME J. Eng. Gas Turbines Power, **128**, pp. 178–182.

[14] GAMBIT 2.4.16 User's Guide.

[15] Gorse, P., Willenborg, K., Busam, S., Ebner, J., Dullenkopf, K., and Wittig, S., 2003, "3D-LDA Measurements in an Aero-Engine Bearing Chamber," ASME Paper No. GT2003-38376.

[16] Launder, B. E., Reece, G. J., and Rodi, W., 1975, "Progress in the Development of a Reynolds-Stress Turbulence Closure," J. Fluid Mech., **68**(3), pp. 537–566.